

Article

Mechanical Properties and Freeze–Thaw Durability of Basalt Fiber Reactive Powder Concrete

Wenjun Li ¹, Hanbing Liu ¹, Bing Zhu ¹, Xiang Lyu ¹ , Xin Gao ² and Chunyu Liang ^{1,*}

¹ College of Transportation, Jilin University, Changchun 130025, China; wenjun18@mails.jlu.edu.cn (W.L.); lhb@jlu.edu.cn (H.L.); zhuhing18@mails.jlu.edu.cn (B.Z.); lvxiang18@mails.jlu.edu.cn (X.L.)

² China Resources Land Limited, Changchun 130025, China; xingao17@mails.jlu.edu.cn

* Correspondence: liangcy@jlu.edu.cn; Tel.: +86-159-4305-9951

Received: 20 July 2020; Accepted: 14 August 2020; Published: 16 August 2020



Abstract: Basalt fiber has a great advantage on the mechanical properties and durability of reactive powder concrete (RPC) because of its superior mechanical properties and chemical corrosion resistance. In this paper, basalt fiber was adopted to modified RPC, and plain reactive powder concrete (PRPC), basalt fiber reactive powder concrete (BFRPC) and steel fiber reactive powder concrete (SFRPC) were prepared. The mechanical properties and freeze–thaw durability of BFRPC with different basalt fiber contents were tested and compared with PRPC and SFRPC to investigate the effects of basalt fiber contents and fiber type on the mechanical properties and freeze–thaw durability of RPC. Besides, the mass loss rate and compressive strength loss rate of RPC under two freeze–thaw conditions (fresh-water freeze–thaw and chloride-salt freeze–thaw) were tested to evaluate the effects of freeze–thaw conditions on the freeze–thaw durability of RPC. The experiment results showed that the mechanical properties and freeze–thaw resistance of RPC increased as the basalt fiber content increase. Compared with the fresh-water freeze–thaw cycle, the damage of the chloride-salt freeze–thaw cycle on RPC was great. Based on the freeze–thaw experiment results, it was found that SFRPC was sensitive to the corrosion of chloride salts and compared with the steel fiber, the improvement of basalt fiber on the freeze–thaw resistance of RPC was great.

Keywords: reactive powder concrete; basalt fiber; chloride-salt corrosion; freeze–thaw durability; mechanical properties

1. Introduction

In the practical application of concrete structural engineering, the deterioration of concrete and the shortening of its service life are related to freeze–thaw damage, chloride ion penetration, sulfate attack and carbonization [1,2]. Accordingly, it is important to improve the durability of concrete structures in practical applications, which is a crucial factor to reduce the cost of infrastructure construction and maintenance. In cold areas, most concrete structures appear in the natural environment, and the freeze–thaw cycle reduces the service life and becomes one of the main sources of damage to the concrete structure [3]. Especially in cold areas, where de-icing salt has been adopted, the concrete damage caused by the coupling action of chloride corrosion and freeze–thaw cycle is serious [4]. The destruction of concrete structures caused by freeze–thaw cycle has aroused widespread concern. The durability of concrete is closely related to the internal pore structure. Concrete structure with low-porosity could effectively reduce the pore solution inside the concrete, thus reducing the internal water pressure caused by the freezing of the pore solution and improving the freeze–thaw resistance of concrete [5]. Besides, the compact concrete structure could hinder the transmission of chloride and greatly reduce the damage caused by chloride ion penetration [6,7].

Reactive powder concrete (RPC), proposed in the 1990s, is an ultra-high-performance concrete characterized by dense microstructure and uniform concrete matrix [8]. The traditional RPC is developed through microstructure enhancement technology and the main improvement is related to matrix uniformity, porosity and microstructure, including eliminating coarse aggregates and reducing the water–binder ratio to improve matrix uniformity [9], optimizing particle gradation to decrease matrix porosity [10] and increasing the silica component by adding silica fume to improve the microstructure of the matrix structure [11]. RPC is seen as a potential material for the field of special prestressed and precast concrete components due to its low permeability, superior mechanical properties and durability [12,13]. Although the manufacturing cost of RPC is generally high, the thickness of concrete component is possible to be reduced due to its ultra-high mechanical properties, resulting in materials and costs saving. Therefore, RPC has certain economic advantages in practical applications [14]. However, RPC still has the characteristics of high brittleness of ordinary concrete and the brittleness of RPC increases as the strength increase. Therefore, the addition of fiber is usually adopted to increase the toughness of RPC [15].

Adding fiber into brittle concrete is a widely used technology. The bridging and pulling effects of fiber could improve the brittleness and impact resistance of the mixture [16,17], and the three-dimensional randomly scattered fiber could effectively inhibit the generation and propagation of cracks [18]. Previous reports have found that polypropylene fiber [19], carbon fiber [20] and steel fiber [21] can be used as reinforcing materials for RPC, and the fiber commonly used to reinforce concrete is steel fiber [22]. To improve the flexural strength, compressive strength, elastic modulus and ductility of RPC, the recommended content of steel fiber is 2% volume fraction [23]. Moreover, adding steel fiber into concrete is judged as an effective method to prevent spalling. However, steel fiber with high content will converge into a spherical shape and the steel fiber is sensitive to chemical corrosion, which results in a decrease in properties of concrete. Besides, adding steel fiber into the concrete will reduce the workability and increase the cost [24].

Basalt fiber is an environmentally friendly and high-performance fiber made of natural volcanic basalt rock, which can be used to reinforce concrete. Due to its excellent acid and alkali resistance, great mechanical properties and high temperature stability, the application prospect of basalt fiber as fiber-reinforced material is broad [25]. Basalt fiber can not only effectively increase the strength and durability of concrete but also has a positive effect on the toughness and crack resistance [26,27]. The excellent reinforcement effect of basalt fiber promotes its application in RPC. Wang et al. [28] researched the effect of basalt fiber on the mechanical properties of high-performance concrete. The results showed that the strength of high-performance concrete increased with the increase in basalt fiber content, and the compressive improved slightly, while flexural strength increased significantly. Grzeszczyk et al. [29] evaluated the effect of basalt fiber content on the mechanical properties of RPC; their results showed that the flexural strength of RPC increased with the increase in basalt fiber content. Liu et al. [30] reported that the basalt fiber could increase the toughness and bending strength of basalt fiber RPC beams, and improve the resistance to steel–concrete interface damage. Most research is about the mechanical properties of basalt fiber-reinforced reactive powder concrete. There is not enough research about the freeze–thaw durability of fiber-reinforced RPC, and the most common fiber in the freeze–thaw durability research of fiber-reinforced RPC is steel fiber [2,31]. Therefore, there are few studies were reported on the effect of basalt fiber on freeze–thaw durability of RPC. Moreover, in cold regions, where de-icing salt has been adopted, the coupling effect of chloride corrosion and freeze–thaw poses a challenge to the application of RPC and, because of the excellent corrosion resistance of basalt fiber, the improvement of basalt fiber on the freeze–thaw durability of RPC is worth exploring. Therefore, it is necessary to investigate the enhancement effect of basalt fiber on the performance of RPC.

In this paper, the mechanical properties and freeze–thaw durability of basalt fiber reactive powder concrete (BFRPC) with different basalt fiber contents (4, 8 and 12 kg/m³) were tested and compared with plain reactive powder concrete (PRPC) and steel fiber reactive powder concrete (SFRPC) to investigate

the impacts of basalt fiber contents and fiber type on the mechanical properties and freeze–thaw durability of RPC. Moreover, the freeze–thaw resistance of RPC under the fresh-water freeze–thaw cycle and the chloride-salt freeze–thaw cycle was tested to investigate the effects of freeze–thaw conditions on the freeze–thaw durability of RPC. The purpose of this paper is to provide a reference for the practical application of BFRPC in cold regions.

2. Materials and Methods

2.1. Materials

Type P.O Portland cement with a strength of 42.5 MPa, manufactured by Yatai Cement Co., Ltd., Jilin, China, was used in this paper. The properties of this cement are given in Table 1. The SF93 silica fume with a specific surface area of 18,100 m²/kg obtained from Si'ao Technology Co., Ltd., Changchun, China, was used in this study. Table 2 shows the chemical composition of silica fume and cement. Three types of quartz sand, with sizes of 20–40, 40–80 and 80–120 mesh, manufactured by Zhenxing quartz sand factory, Luoyang, were used. The proportion of three types of quartz sand was 2:2:1. The quartz powder (400 mesh) was used to fill micro pores. The chemical composition of quartz sand is given in Table 3. HPWR-Q8011 polycarboxylic superplasticizer (water reduction rate 25%) obtained from Qinfen Building Materials Co., Ltd., Shanxi, China, was used to prepare all tested concrete. Chopped basalt fiber, produced by Anjie Composite Material Co., Ltd., Haining, China, was used to reinforce RPC in this study and the properties of basalt fiber are shown in Table 4. Steel fiber with a length of 13 mm and a diameter of 200 µm was adopted in this paper, obtained from Daxing Matel Fiber Co., Ltd., Ganzhou, China, which had a tensile strength of 2850 MPa. The appearance of basalt fiber and steel fiber is given in Figure 1. The tap water was used as mixed water.

Table 1. Basic properties of cement.

Density (kg/m ³)	Specific Surface Area (m ² /kg)	Setting Time (min)		Compressive Strength (MPa)	Flexural Strength (MPa)
		Initial Setting	Final Setting		
3160	385	91	145	62.2	9.1

Table 2. The chemical composition of cement and silica fume.

Material	Chemical Composition (%)					
	SiO ₂	Al ₂ O ₃	Fe ₂ O ₃	CaO	MgO	SO ₃
Cement	22.60	5.60	4.30	62.70	1.70	2.50
Silica fume	93.3	0.73	0.49	0.85	1.21	1.02

Table 3. The chemical composition of quartz sand.

Material	Chemical Composition (%)					
	SiO ₂	Fe	Al ₂ O ₃	K ₂ O	Na ₂ O	H ₂ O
Quartz Sand	99.68	0.0062	0.0122	0.0011	0.002	0.02

Table 4. The performance indicator of basalt fiber.

Type	Length (mm)	Diameter (µm)	Linear Density (tex)	Tensile Strength (MPa)	Elastic Modulus (GPa)	Breaking Strength (N/tex)	Elongation (%)
Basalt fiber	22	23	2392	2836	62	0.69	3



Figure 1. Fiber: (a) Basalt fiber (b) Steel fiber.

2.2. Mixture Proportion and Specimen Preparation

The best mixture proportion of RPC was obtained from the response surface method in our group's previous study [32], and based on the optimal mixture proportion; basalt fiber and steel fiber were added into RPC with an external mixing method. The content of basalt fiber was 4, 8 and 12 kg/m³, respectively. The content of steel fiber was 2% volume fraction [23]. Moreover, PRPC specimens without fiber were prepared as the control group to investigate the effects of basalt fiber and steel fiber on the mechanical properties and freeze–thaw durability of RPC. The mixture proportion of BFRPC and SFRPC is shown in Table 5.

Table 5. The mixture proportion of basalt fiber reactive powder concrete (BFRPC) and steel fiber reactive powder concrete (SFRPC).

Mix ID	Basalt Fiber (kg/m ³)	Steel Fiber (%)	Cement (kg/m ³)	Quartz Sand (kg/m ³)	Silica Fume (kg/m ³)	Quartz Powder (kg/m ³)	Water (kg/m ³)	Water Reducer (kg/m ³)
R	-	-	834.73	939.03	208.68	308.85	166.95	52.17
BF4	4	-	834.73	939.03	208.68	308.85	166.95	52.17
BF8	8	-	834.73	939.03	208.68	308.85	166.95	52.17
BF12	12	-	834.73	939.03	208.68	308.85	166.95	52.17
SF	-	2	834.73	939.03	208.68	308.85	166.95	52.17

All RPC mixtures were prepared by using an ISO 679 mixer with a capacity of 5 L. The degree of dispersion of basalt fiber and steel fiber in the mixture has a significant impact on the properties of RPC. During the process of mixing, the fibers were put into the mixer step by step to ensure the dispersion of fibers. The specific of mixing were as follows. (1) Put the quartz sand and fiber into the mixer and mix for 2 min. The friction between the quartz sand particles makes the fiber evenly dispersed. (2) Put the cement, quartz powder and silica fume into the mixer and mix for 3 min. (3) Dissolve the polycarboxylic superplasticizer into the water and add the solution into the mixer in two lots, mixing for 3 min each time. After stirring, the mixture was filled into a metal mold with a size of 40 × 40 × 160 mm, immediately, and compressed by vibrating on the ZT-96 vibrator table. The specimens were placed in an environment of 95% humidity and 20 °C for 24 h and then de-moulded. The specimens were cured for 48 h under the condition of 90 °C steam curing, the heating speed was 12 °C/h and the cooling speed was 15 °C/h.

2.3. Testing Methods

2.3.1. Flexural Strength

According to the three-point flexural test described in Chinese national standard GB/T 17671-1999 [33] to evaluate the flexural strength of RPC. The distance between the two fulcrum points was 100 mm. The specimens were placed with the side face up in the testing machine and align the center line of the specimens with the upper fixture. The loading speed was set to 50 N/s. Three specimens with volumes of 40 × 40 × 160 mm were made in each group for testing and the mean of the three measured results was used as the flexural strength. The specific calculation process is shown in Formula (1). The specific experimental device of flexural strength is shown in Figure 2.

$$f_f = \frac{1.5F_f L}{b^3} \quad (1)$$

where f_f refers to the flexural strength of specimens (MPa), F_f refers to the failure load (N), L refers to the distance between the two fulcrum and $L = 100$ mm, b refers to the cross-sectional width of the specimens and $b = 40$ mm.

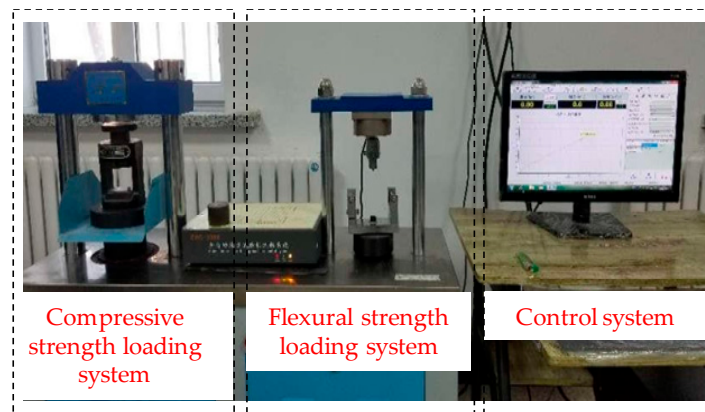


Figure 2. The specific experimental device.

2.3.2. Compressive Strength

According to the Chinese national standard GB/T 17671-1999 [33] to evaluate the compressive strength of RPC. The six fracture blocks obtained after the flexural strength test were adopted for the compressive strength test. Removed the debris on the surface of the fracture blocks and placed it in the fixture. The two sides of the fracture blocks were used as the compression surface. Adjusted the position of the specimen so that the compression surface and the fixture were in full contact. The loading rate was set to 2.4 kN/s. The compressive strength of RPC was the mean of the six measured results. The specific calculation process is shown in Formula (2). The specific experimental device of compressive strength is shown in Figure 2.

$$f_c = \frac{F}{A} \quad (2)$$

where f_c refers to the compressive strength of RPC (MPa), F refers to the failure load (N), A refers to the compression surface and $A = 1600$ mm².

2.3.3. Freeze–Thaw Cycle

In this paper, the freeze–thaw durability of PRPC, SFRPC and BFRPC under two freeze–thaw conditions was investigated. The specific freeze–thaw cycle test grouping is shown in Table 6. According

to the rapid freeze–thaw method described in Chinese national standard GB/T50082-2009 [34] to investigate the freeze–thaw durability of PRPC, SFRPC and BFRPC. The freezing temperature is $-18 \pm 2 \text{ }^\circ\text{C}$ and the freezing time is 3 h. The melting temperature is $5 \pm 2 \text{ }^\circ\text{C}$ and the melting time is greater than one quarter of the entire freezing and melting cycle time. The specific arrangement of the freeze–thaw cycle test is shown in Figure 3.

Table 6. Freeze–thaw cycle test grouping.

Mix ID	WR	WBF12	WSF	NR	NBF4	NBF8	NBF12	NSF
Freeze–thaw medium	fresh water	fresh water	fresh water	5 wt% NaCl				

Note: W refers to fresh water, N refers to 5 wt% NaCl solution.

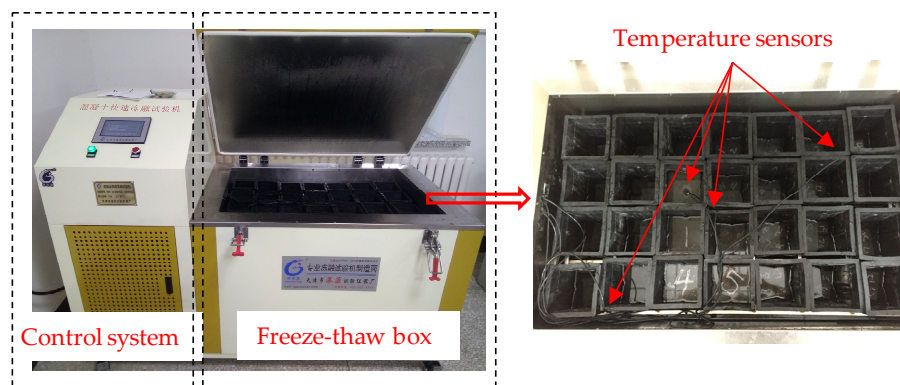


Figure 3. Freeze–thaw cycle test.

The cured specimens were immersed in fresh water and 5 wt% NaCl solution for 48 h. The groups of WR, WB12 and WS were immersed in fresh water and the groups of NR, NB4, NB8, NB12 and NS were immersed in 5 wt% NaCl solution. After immersion for 48 h, the the moisture on the surface of the specimens wiped off; the initial mass of the specimens was weighed and the initial compressive strength was measured. Then, the remaining specimens were put into the freeze–thaw test machine and injected fresh water and 5 wt% NaCl solution until the water level was 5 cm above the top surface of the specimens. The number of freeze–thaw cycle was set to 800, and the mass and compressive strength of the specimens were measured every 100 cycles. The mass loss rate and compressive strength loss rate were adopted to investigate the freeze–thaw durability of BFRPC and SFRPC. The specific calculation formulas are as follows:

$$MR = \frac{M_i - M_0}{M_0} \times 100\% \tag{3}$$

$$CR = \frac{f_{Ci} - f_{C0}}{f_{C0}} \times 100\% \tag{4}$$

where *MR* refers to the mass loss rate, *M_i* refers to the mass at the Nth cycles, *M₀* refers to the initial mass, *CR* refers to the compressive strength loss rate, *f_{Ci}* refers to the compressive strength at the Nth cycles, *f_{C0}* refers to the initial compressive strength.

3. Results and Discussion

3.1. Mechanical Properties

In this paper, the mechanical properties of BFRPC with different basalt fiber contents were tested and compared with PRPC and SFRPC to evaluate the effects of basalt fiber contents and fiber type on the mechanical properties of RPC.

3.1.1. Compressive Strength

Figure 4 shows that the effects of basalt fiber contents and fiber type on the compressive strength of RPC. It can be known from Figure 4 that the addition of basalt fiber could improve the compressive strength of RPC and the compressive strength of RPC increases with the increase in basalt fiber content, which is consistent with the conclusion of Wang et al. [28]. When the basalt fiber content is 12 kg/m^3 , the compressive strength of BFRPC reaches the maximum value of 149.40 MPa, which is 6% higher than that of PRPC. Liu et al. [35] pointed out that evenly distributed basalt fiber inside the RPC could inhibit the initiation of cracks and bear part of the load, thus improving the compressive strength of RPC. Besides, basalt fiber is composed of oxides such as silica, alumina and magnesia, and its chemical composition is similar to cement. The bond strength between basalt fiber and cement paste is great [36], thus improving the compressive strength of RPC. Compared with SFRPC, the compressive strength of BFRPC with a basalt fiber content of 12 kg/m^3 is 4.3% lower, which indicates that basalt fiber is not as effective as steel fiber in improving the compressive strength of RPC.

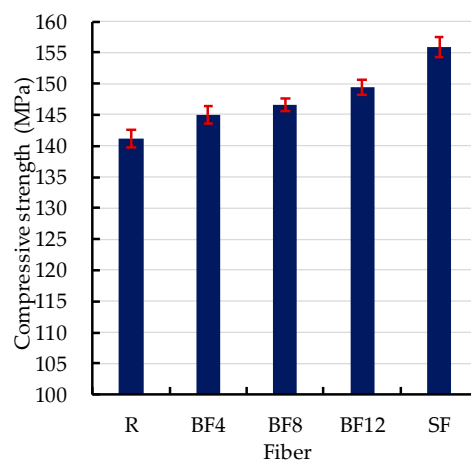


Figure 4. Effect of basalt fiber content and fiber type on the compressive strength of RPC.

3.1.2. Flexural Strength

The experiment result of the flexural strength test is shown in Figure 5. Figure 5 shows that the flexural strength of RPC increases as the basalt fiber content increases, which is the same as the improvement of basalt fiber on the compressive strength. The increased trend of flexural strength is a slightly different from that of compressive strength. Compared with compressive strength, when the basalt fiber is from 8 to 12 kg/m^3 , a significant increase in flexural strength of BFRPC occurs and the flexural strength of BFRPC reaches 16.23 MPa, which is 18.5% higher than that of PRPC. Compared with compressive strength, the improvement of basalt fiber on the flexural strength of RPC is greater, aggregating with the conclusion conducted by Wang et al. [28]. The improvement of the flexural strength of BFRPC is related to the uniform distribution of basalt fiber inside the RPC. The uniform distributed basalt fiber could inhibit the generation and propagation of cracks and bear part of the stress, reducing the stress concentration near the crack and redistributing the stress [16], thus improving the flexural strength of RPC. Besides, the basalt fiber inside the RPC submits a three-dimensional random distribution; this distribution system can limit the deformation of RPC under loading conditions, which leads to an increase in the flexural strength of RPC. The three-dimensional distribution system of basalt fiber is gradually improved as the basalt fiber content increase, which is reflected in the significant increase in flexural strength of BFRPC with a basalt fiber content of 12 kg/m^3 . Moreover, comparing the flexural strength of SFRPC with that of BFRPC (12 kg/m^3 content), it can be known that the flexural strength of BFRPC and SFRPC is similar, which indicates that when the basalt fiber content is 12 kg/m^3 , the reinforcement effect of basalt fiber on the flexural strength of RPC is about same as steel fiber; Branston et al. [25] reported a similar conclusion.

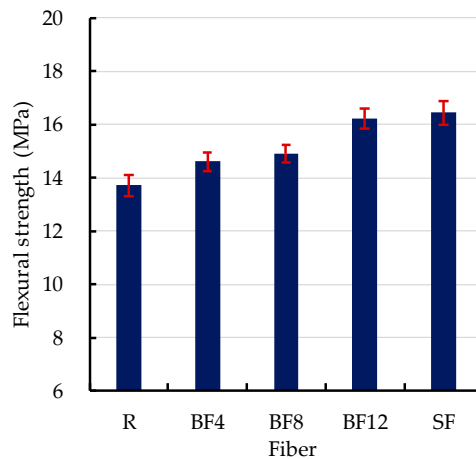


Figure 5. Effect of basalt fiber content and fiber type on the flexural strength of RPC.

3.2. Effect of Fiber on Freeze–Thaw Durability of RPC

3.2.1. Mass Loss

The mass loss of BFRPC with different basalt fiber contents was tested under the chloride–salt freeze–thaw cycle and compared with the PRPC and SFRPC to evaluate the effects of basalt fiber contents and fiber type on the freeze–thaw durability of RPC. Figure 6 shows that the effects of basalt fiber contents and fiber type on the mass loss of RPC. It can be known from Figure 6 that the mass loss rate of RPC increases with the increase in the number of freeze–thaw cycles. The mass loss of RPC is mainly caused by surface scaling and the edges of the specimen surface will fall off as the freeze–thaw cycle test continue, resulting in fiber exposure [2]. It is worth noting that the mass loss rate of BFRPC (8 and 12 kg/m³ content) is negative in the initial part of the freeze–thaw test, which is related to the water absorption of basalt fiber. In the initial part of the freeze–thaw test, the mass of water absorbed by the basalt fiber is greater than that of the surface scaling of RPC caused by freeze–thaw damage. When freeze–thaw cycle levels are the same, the mass loss rate of RPC decreases as the basalt fiber content increase, which indicates that the basalt fiber could improve the freeze–thaw resistance. When the number of freeze–thaw cycles is less than 600, the mass loss rate of SFRPC is in a stable increase stage and the mass loss is mainly caused by surface scaling. When it exceeds 600, a significant increase in the mass loss rate occurs, and the reason is that the steel fiber exposed to the chloride ion environment corrodes rapidly, thus leading to more peeling off the edge of the specimen surface. The mass loss rate of SFRPC reaches 3.03% after 800 freeze–thaw cycles, which is higher than that of BFRPC. This indicates that steel fiber is not as effective as basalt fiber in improving the freeze–thaw durability of RPC.

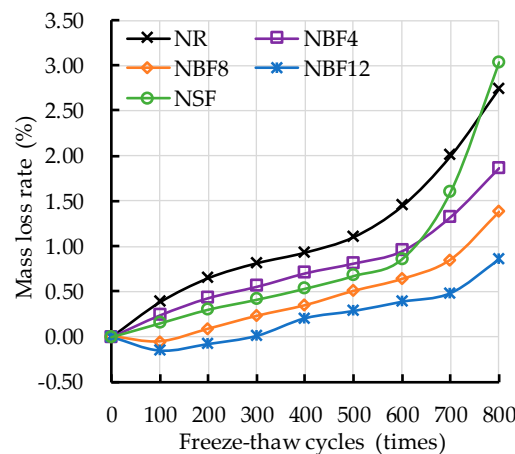


Figure 6. Mass loss rate versus freeze–thaw cycles.

3.2.2. Compressive Strength Loss

The compressive strength of BFRPC with different basalt fiber contents was tested under the chloride-salt freeze–thaw cycle and the compressive strength loss rate was calculated by Formula (4), and compared with the PRPC and SFRPC to evaluate the impacts of basalt fiber contents and fiber type on the freeze–thaw durability of RPC.

The compressive strength and compressive strength loss rate vs. freeze–thaw cycles are shown in Figure 7. It can be seen from Figure 7a that, for all RPC specimens, the compressive strength of RPC decreases as the freeze–thaw test continues, which indicates that the freeze–thaw durability of RPC gradually deteriorates under the chloride-salt freeze–thaw cycle. During the freeze–thaw test, the frost expansion of the pore solution inside the RPC leads to the initiation of micro cracks, thus reducing the compressive strength of RPC, which is consistent with the conclusion reported by An et al. [31]. Comparing the compressive strength of SFRPC with that of BFRPC (12 kg/m³ content), it can be known that the decline in the compressive strength of SFRPC is higher and the compressive strength of SFRPC and BFRPC is almost the same after 800 freeze–thaw cycles, which indicates that the corrosion of steel fiber not only increases the mass loss of RPC, but also has a negative effect on the compressive strength of RPC. It can be seen from Figure 7b that, for PRPC, BFRPC and SFRPC specimens, the compressive strength loss rate increases as the freeze–thaw test continues. At all freeze–thaw cycle levels, the compressive strength loss rate of BFRPC is lower than that of PRPC, and the higher the basalt fiber content, the lower the compressive strength loss rate of BFRPC, which indicates that adding basalt fiber could improve the freeze–thaw durability of RPC. This is because the addition of basalt fiber increases the number of harmless pores which could effectively reduce the freezing pressure of the pore solution, thus improving the freeze–thaw durability of RPC [37]. Moreover, comparing the compressive strength loss rate of SFRPC with that of BFRPC, the compressive strength loss rate of BFRPC (8 and 12 kg/m³ content) is lower than that of SFRPC throughout the freeze–thaw cycle test. It indicates that steel fiber is not as effective at enhancing the freeze–thaw resistance of RPC as basalt fiber.

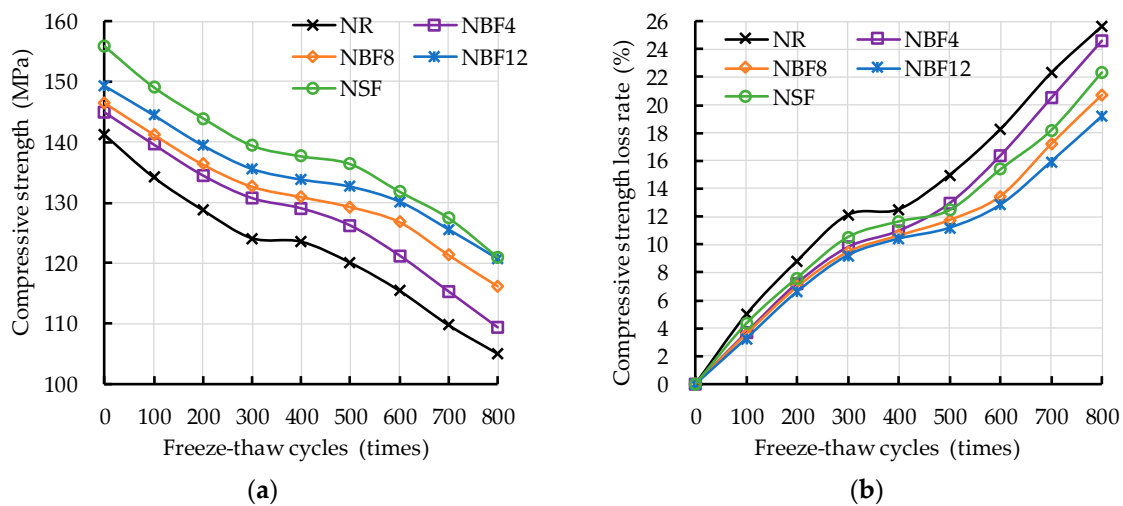


Figure 7. Compressive strength and compressive strength loss rate versus freeze–thaw cycles: (a) Compressive strength; (b) Compressive strength loss rate.

3.3. Effect of Freeze–Thaw Condition on the Freeze–Thaw Durability of RPC

3.3.1. Mass Loss

The mass loss of RPC was tested under two freeze–thaw conditions and the mass loss rate was calculated by Formula (3) to evaluate the effects of freeze–thaw conditions on the freeze–thaw durability of RPC. The mass loss rate vs. freeze–thaw cycles is shown in Figure 8. This figure shows that the mass loss rate of RPC increases as the freeze–thaw cycle test continues, and the presence of basalt

fiber water absorption leads to a negative value of the mass loss rate of BFRPC in the early stage of the freeze–thaw test; as the density of the 5-wt% NaCl solution is greater than that of fresh water, when the number of freeze–thaw cycles is less than 300, the mass loss rate of BFRPC (chloride-salt freeze–thaw) is lower than that of BFRPC (fresh-water freeze–thaw). Compared with the fresh-water freeze–thaw cycle, the mass loss rate of RPC is higher under the chloride-salt freeze–thaw cycle, it can be known that chloride-salt freeze–thaw cycles causes more surface scaling, which indicates that the chloride-salt freeze–thaw cycle accelerates the deterioration of the freeze–thaw durability of RPC. After 800 freeze–thaw cycles, the mass loss rate of BFRPC under two freeze–thaw conditions is less than 1%. Besides, at all freeze–thaw cycle levels, the difference in mass loss rate of BFRPC under two freeze–thaw conditions is less than 0.25%. This indicates that the basalt fiber could significantly improve the freeze–thaw durability and chloride ion resistance of RPC.

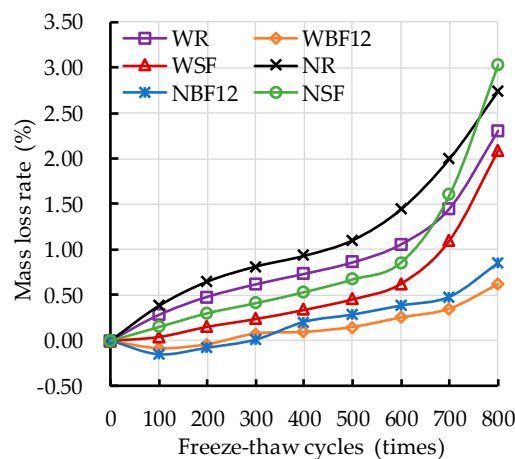


Figure 8. Mass loss versus freeze–thaw cycles.

3.3.2. Compressive Strength Loss

The compressive strength of RPC was tested under two freeze–thaw conditions and the compressive strength loss rate was calculated by Formula (4) to evaluate the effects of freeze–thaw conditions on the freeze–thaw durability of RPC.

The compressive strength and its loss rate vs. freeze–thaw cycles are shown in Figure 9. Figure 9a shows that, for all RPC mixtures, the compressive strength of RPC decreases with the freeze–thaw test continues. Before the freeze–thaw test, the compressive strength of RPC soaked in 5 wt% NaCl solution for 48 h is lower than that of RPC soaked in water, which shows that the immersion of 5 wt% NaCl solution has a certain negative effect on the compressive strength of RPC. When the number of freeze–thaw cycles is the same, the compressive strength of RPC under chloride-salt freeze–thaw cycle is lower than that of RPC under fresh-water freeze–thaw cycle, which indicates that compared with the fresh-water freeze–thaw cycle, chloride-salt freeze–thaw cycle causes greater damage to RPC, similar conclusion is reported by Vaitkevičius et al. [38]. It can be seen from Figure 9b that the compressive strength loss rate of RPC increases as the freeze–thaw cycles increase. At all freeze–thaw cycle levels, compared with the RPC under fresh-water freeze–thaw cycle, the compressive strength loss rate of RPC under chloride-salt freeze–thaw cycle is higher. Due to freeze–thaw cycle, the pore cracked and the microcracks generated provide channels for further penetration of chloride ions. Therefore, the coupling effect of freeze–thaw cycle and chloride ion erosion has more aggressive impact on the durability of RPC [2,39]. After 800 freeze–thaw cycles, the compressive strength loss rate of BFRPC under two freeze–thaw conditions is less than 20% and the difference in compressive strength loss rate of BFRPC under two freeze–thaw conditions is less than 0.9%. It indicates that the basalt fiber could significantly improve the freeze–thaw durability and chloride ion resistance of RPC and the conclusion is consistent with the mass loss rate test.

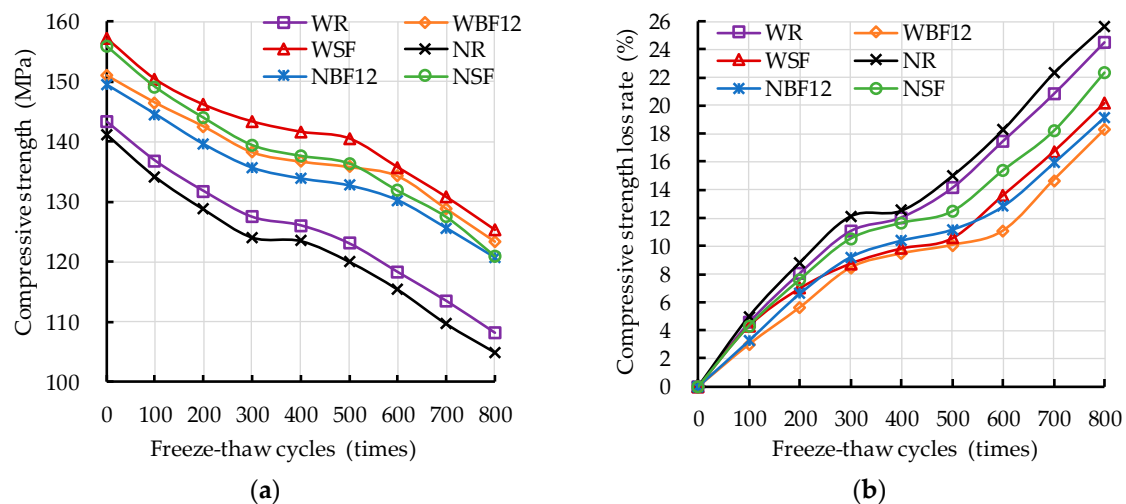


Figure 9. Compressive strength and Compressive strength loss rate versus freeze–thaw cycles: (a) Compressive strength; (b) Compressive strength loss rate.

4. Conclusions

In this paper, the mechanical properties and freeze–thaw durability of BFRPC with different basalt fiber contents were tested and compared with PRPC and SFRPC to investigate the effects of basalt fiber contents and fiber type on the mechanical properties and freeze–thaw durability of RPC. Besides, the freeze–thaw durability of RPC under two freeze–thaw conditions was tested to investigate the effects of freeze–thaw conditions on the freeze–thaw durability of RPC. Based on the results of the experiment, the conclusions are as follows:

1. The compressive strength and flexural strength can be improved by adding basalt fiber into RPC, and the compressive and flexural strength of BFRPC increase as the basalt fiber content increases. Compared with PRPC, the compressive strength and flexural strength of BFRPC (12 kg/m^3 content) are increased by 6% and 18.5%, respectively; the improvement of basalt fiber on the flexural strength of RPC is greater than compressive strength.
2. The freeze–thaw durability of BFRPC increases as the basalt fiber content increases. After 800 freeze–thaw cycles, the mass loss rate and compressive strength loss rates of BFRPC with a basalt fiber content of 12 kg/m^3 are 0.85% and 19.17%, respectively, which are lower than that of PRPC. The addition of basalt fiber could significantly improve the freeze–thaw durability of RPC.
3. Compared with the fresh-water freeze–thaw cycle, the mass loss rate and compressive strength loss rate of RPC are higher under the chloride-salt freeze–thaw cycle, and the damage of the chloride-salt freeze–thaw cycle on RPC is great.
4. After 800 freeze–thaw cycles, the mass loss rate and compressive strength loss rates of SFRPC are greater than 2% and 20%, respectively, which are higher than that of BFRPC. Steel fiber is not as effective at enhancing the freeze–thaw durability of RPC as basalt fiber.

Author Contributions: Conceptualization, H.L. and X.G.; methodology, C.L. and X.G.; formal analysis, W.L. and X.L.; investigation, W.L., B.Z. and X.L.; writing—original draft preparation, W.L.; writing—review and editing, C.L.; funding acquisition, H.L. All authors have read and agreed to the published version of the manuscript.

Funding: This research was funded by the Industrial Technology Research & Development Special Project of Jilin Province (2018C042-1); the Transportation Science and Technology Program of Jilin Province (2018-1-9); and the Science Technology Development Program of Jilin Province (20200403157SF).

Acknowledgments: The authors would like to express their appreciation to the anonymous reviewers for their constructive suggestions and comments on improving the quality of the paper.

Conflicts of Interest: The authors declare no conflict of interest.

References

1. Glasser, F.P.; Marchand, J.; Samson, E. Durability of concrete—Degradation phenomena involving detrimental chemical reactions. *Cem. Concr. Res.* **2008**, *38*, 226–246. [[CrossRef](#)]
2. Wang, Y.; An, M.Z.; Yu, Z.R.; Han, S.; Ji, W.Y. Durability of reactive powder concrete under chloride-salt freeze–thaw cycling. *Mater. Struct.* **2017**, *50*, 18. [[CrossRef](#)]
3. Wang, Y.R.; Cao, Y.B.; Zhang, P.; Ma, Y.W.; Zhao, T.J.; Wang, H.; Zhang, Z.H. Water absorption and chloride diffusivity of concrete under the coupling effect of uniaxial compressive load and freeze-thaw cycles. *Constr. Build. Mater.* **2019**, *209*, 566–576. [[CrossRef](#)]
4. Sun, W.; Mu, R.; Luo, X.; Miao, C.W. Effect of chloride salt, freeze–thaw cycling and externally applied load on the performance of the concrete. *Cem. Concr. Res.* **2002**, *32*, 1859–1864. [[CrossRef](#)]
5. Cai, H.; Liu, X. Freeze-thaw durability of concrete: Ice formation process in pores. *Cem. Concr. Res.* **1998**, *28*, 1281–1287. [[CrossRef](#)]
6. Liu, Z.Y.; Zhang, Y.S.; Jiang, Q. Continuous tracking of the relationship between resistivity and pore structure of cement pastes. *Constr. Build. Mater.* **2014**, *53*, 26–31. [[CrossRef](#)]
7. Wang, L.C.; Ueda, T. Mesoscale Modeling of Chloride Penetration in Unsaturated Concrete Damaged by Freeze-Thaw Cycling. *J. Mater. Civ. Eng.* **2014**, *26*, 955–965. [[CrossRef](#)]
8. Richard, P.; Cheyrezy, M. Composition of reactive powder concretes. *Cem. Concr. Res.* **1995**, *25*, 1501–1511. [[CrossRef](#)]
9. Chan, Y.W.; Chu, S.H. Effect of silica fume on steel fiber bond characteristics in reactive powder concrete. *Cem. Concr. Res.* **2004**, *34*, 1167–1172. [[CrossRef](#)]
10. Bonneau, O.; Vernet, C.; Moranville, M.; Aitcin, P.C. Characterization of the granular packing and percolation threshold of reactive powder concrete. *Cem. Concr. Res.* **2000**, *30*, 1861–1867. [[CrossRef](#)]
11. Mostofinejad, D.; Nikoo, M.R.; Hosseini, S.A. Determination of optimized mix design and curing conditions of reactive powder concrete (RPC). *Constr. Build. Mater.* **2016**, *123*, 754–767. [[CrossRef](#)]
12. Yazıcı, H.; Yardımcı, M.Y.; Aydın, S.; Karabulut, A.S. Mechanical properties of reactive powder concrete containing mineral admixtures under different curing regimes. *Constr. Build. Mater.* **2009**, *23*, 1223–1231. [[CrossRef](#)]
13. Long, G.C.; Wang, X.Y.; Xie, Y.J. Very-high-performance concrete with ultrafine powders. *Cem. Concr. Res.* **2002**, *32*, 601–605. [[CrossRef](#)]
14. Yazıcı, H.; Yardımcı, M.Y.; Yiğiter, H.; Aydın, S.; Türkel, S. Mechanical properties of reactive powder concrete containing high volumes of ground granulated blast furnace slag. *Cem. Concr. Compos.* **2010**, *32*, 639–648. [[CrossRef](#)]
15. Afrouhsabet, V.; Biolzi, L.; Ozbakkaloglu, T. High-performance fiber-reinforced concrete: A review. *J. Mater. Sci.* **2016**, *51*, 6517–6551. [[CrossRef](#)]
16. Al-Masoodi, A.H.H.; Kawan, A.; Kasmuri, M.; Hamid, R.; Khan, M.N.N. Static and dynamic properties of concrete with different types and shapes of fibrous reinforcement. *Constr. Build. Mater.* **2016**, *104*, 247–262. [[CrossRef](#)]
17. Zhou, W.; Hu, H.B.; Zheng, W.Z. Bearing capacity of reactive powder concrete reinforced by steel fibers. *Constr. Build. Mater.* **2013**, *48*, 1179–1186. [[CrossRef](#)]
18. Al-Tikrite, A.; Hadi, M.N.S. Stress–Strain Relationship of Unconfined RPC Reinforced with Steel Fibers under Compression. *J. Mater. Civ. Eng.* **2018**, *30*, 04018234. [[CrossRef](#)]
19. Hiremath, P.N.; Yaragal, S.C. Performance evaluation of reactive powder concrete with polypropylene fibers at elevated temperatures. *Constr. Build. Mater.* **2018**, *169*, 499–512. [[CrossRef](#)]
20. Wang, H.; Gao, X.J.; Liu, J.Z.; Ren, M.; Lu, A.X. Multi-functional properties of carbon nanofiber reinforced reactive powder concrete. *Constr. Build. Mater.* **2018**, *187*, 699–707. [[CrossRef](#)]
21. Tai, Y.S.; Pan, H.H.; Kung, Y.N. Mechanical properties of steel fiber reinforced reactive powder concrete following exposure to high temperature reaching 800 °C. *Nucl. Eng. Des.* **2011**, *241*, 2416–2424. [[CrossRef](#)]
22. Scheinherrová, L.; Vejmelková, E.; Keppert, M.; Bezdička, P.; Doleželová, M.; Krejsová, J.; Grzeszczyk, S.; Matuszek-Chmurowska, A.; Černý, R. Effect of Cu-Zn coated steel fibers on high temperature resistance of reactive powder concrete. *Cem. Concr. Res.* **2019**, *117*, 45–57. [[CrossRef](#)]
23. Scrivener, K.L.; Kirkpatrick, R.J. Innovation in use and research on cementitious material. *Cem. Concr. Res.* **2008**, *38*, 128–136. [[CrossRef](#)]

24. Olivito, R.S.; Zuccarello, F.A. An experimental study on the tensile strength of steel fiber reinforced concrete. *Compos. Part B Eng.* **2010**, *41*, 246–255. [[CrossRef](#)]
25. Branston, J.; Das, S.; Kenno, S.Y.; Taylor, C. Mechanical behaviour of basalt fibre reinforced concrete. *Constr. Build. Mater.* **2016**, *124*, 878–886. [[CrossRef](#)]
26. Algin, Z.; Ozen, M. The properties of chopped basalt fibre reinforced self-compacting concrete. *Constr. Build. Mater.* **2018**, *186*, 678–685. [[CrossRef](#)]
27. Kizilkanat, A.B.; Kabay, N.; Akyüncü, V.; Chowdhury, S.; Akça, A.H. Mechanical properties and fracture behavior of basalt and glass fiber reinforced concrete: An experimental study. *Constr. Build. Mater.* **2015**, *100*, 218–224. [[CrossRef](#)]
28. Wang, D.H.; Ju, Y.Z.; Shen, H.; Xu, L.B. Mechanical properties of high performance concrete reinforced with basalt fiber and polypropylene fiber. *Constr. Build. Mater.* **2019**, *197*, 464–473. [[CrossRef](#)]
29. Grzeszczyk, S.; Matuszek-Chmurowska, A.; Vejmelková, E.; Černý, R. Reactive Powder Concrete Containing Basalt Fibers: Strength, Abrasion and Porosity. *Materials* **2020**, *13*, 2948. [[CrossRef](#)]
30. Liu, H.; Lyu, X.; Zhang, Y.; Luo, G.; Li, W. Bending Resistance and Failure Type Evaluation of Basalt Fiber RPC Beam Affected by Notch and Interfacial Damage Using Acoustic Emission. *Appl. Sci.* **2020**, *10*, 1138. [[CrossRef](#)]
31. An, M.Z.; Wang, Y.; Yu, Z.R. Damage mechanisms of ultra-high-performance concrete under freeze–thaw cycling in salt solution considering the effect of rehydration. *Constr. Build. Mater.* **2019**, *198*, 546–552. [[CrossRef](#)]
32. Liu, H.; Liu, S.; Wang, S.; Gao, X.; Gong, Y. Effect of Mix Proportion Parameters on Behaviors of Basalt Fiber RPC Based on Box-Beam Model. *Appl. Sci.* **2019**, *9*, 2031. [[CrossRef](#)]
33. Quality and Technology Supervision Bureau of the People’s Republic of China. *Method of Testing Cements—Determination of Strength*; Quality and Technology Supervision Bureau of the People’s Republic of China: Beijing, China, 1999. (In Chinese)
34. Ministry of Housing and Urban-Rural Construction of the People’s Republic of China. *Standard for Test Methods of Long-Term Performance and Durability of Ordinary Concrete*; Ministry of Housing and Urban-Rural Construction of the People’s Republic of China: Beijing, China, 2009. (In Chinese)
35. Liu, H.; Liu, S.; Zhou, P.; Zhang, Y.; Jiao, Y. Mechanical Properties and Crack Classification of Basalt Fiber RPC Based on Acoustic Emission Parameters. *Appl. Sci.* **2019**, *9*, 3931. [[CrossRef](#)]
36. Rybin, V.A.; Utkin, A.V.; Baklanova, N.I. Alkali resistance, microstructural and mechanical performance of zirconia-coated basalt fibers. *Cem. Concr. Res.* **2013**, *53*, 1–8. [[CrossRef](#)]
37. Zhao, Y.R.; Wang, L.; Lei, Z.K.; Han, X.F.; Shi, J.N. Study on bending damage and failure of basalt fiber reinforced concrete under freeze-thaw cycles. *Constr. Build. Mater.* **2018**, *163*, 460–470. [[CrossRef](#)]
38. Vaitkevičius, V.; Šerelis, E.; Rudžionis, Ž. Nondestructive testing of ultra-high performance concrete to evaluate freeze-thaw resistance. *Mechanika* **2012**, *18*, 164–169. [[CrossRef](#)]
39. Zhou, Z.D.; Qiao, P.Z. Durability of ultra-high performance concrete in tension under cold weather conditions. *Cem. Concr. Compos.* **2018**, *94*, 94–106. [[CrossRef](#)]

